# Chapter 4

# Carbon nanotube

# fabrication and devices

## 4.1 History and properties of carbon nanotubes

Carbon nanotubes (CNT's) were first discovered in 1991 by Ijima[1], who found a nested form of CNT know as a multi-walled nanotube (MWNT). Soon after, in 1993, Ijima and Ichihashi[2] as well as Bethune[3] et al. discovered that under the proper conditions one can produce single-walled nanotubes (SWNT's), which can have dimensions as small as .4 nm.[4] Since then, CNT's have been an extremely active area of scientific research. Mechanically, CNT's have an unprecedented degree of tensile strength and reversible deformability. Electrically, this material can exhibit or lack a band gap. Due to these interesting properties, nanotubes have been integrated in devices such as transistors[5], room-temperature single-electron transistors (SET's)[6], atomic force microscope tips[7] and other mechanical structures.[8] There have been uses proposed such as nearly frictionless nano-bearings[9], mechanical memory arrays[10], and more fancifully, a space elevator.

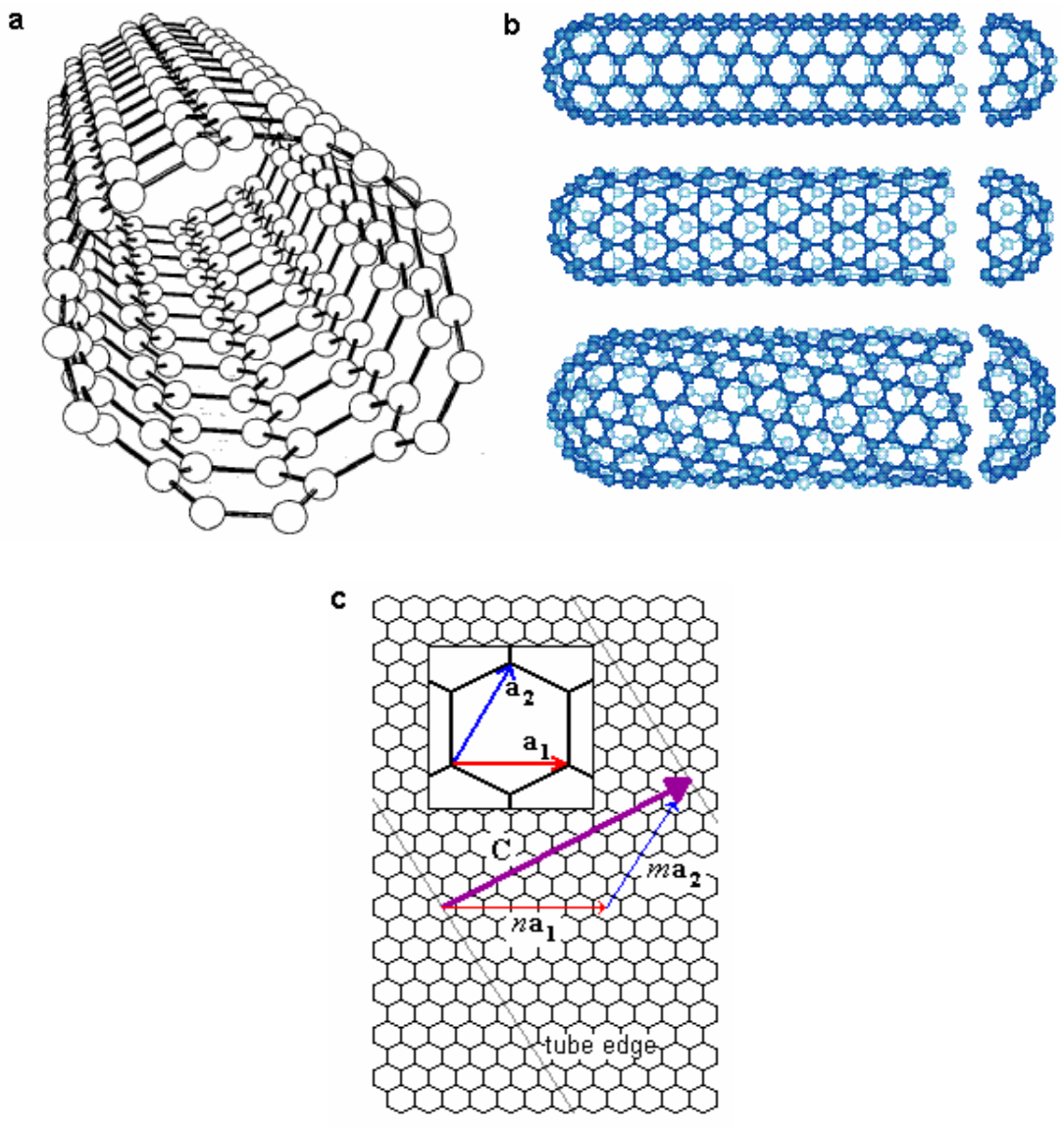


Figure 4.1: Basics of carbon nanotube structure. **a**, hexagonal, $sp^2$-bonded carbon rings comprise the length of the nanotube. **b**, single-walled nanotubes of various chiralities with endcaps. **c**, vector definition of nanotube chirality (inset: basis vectors $\mathbf{a_1}$ and $\mathbf{a_2}$).

The atomic structure of SWNT's can be understood by beginning with graphite's atomic structure of repeating units of hexagonal rings, which has a $sp^2$ bonding structure. A SWNT is formed by rolling up a graphene sheet into a tube, as shown in Figure 4.1a. The ends are capped with hemispherical carbon bonded in hexagonal and pentagonal

rings similar to a soccer ball (Figure 4.1b). Another way to think of a SWNT is as an extended fullerene, of which the "bucky ball" ($C_{60}$) is the most famous.[11] As mentioned above, CNT's come in two "flavors": single-walled nanotubes and multi-walled nanotubes, the latter of which are comprised of multiple nested SWNT's. SWNT's are typically several nanometers in diameter and have been synthesized in lengths up to several hundred microns.[12]

Nanotubes have a variety of interesting and useful properties. In the mechanical regime, they are predicted to have a very large Young's modulus, approximately 1 TPa,[13] greater than that of steel. The large Young's modulus makes CNT's highly desirable for nano-scale resonators, as explained later in this chapter. Carbon nanotubes also have the capability to buckle and restore their shape and are stable to 2800°C in vacuum and 750°C in air.[14] Their robustness and small size make CNT's a nearly ideal source for field emission of electrons[15], an effect that will be described in more detail later.

The particular direction and length of the rolling vector, known as the helicity or chirality of the nanotube, has a profound impact on the electrical properties of a SWNT. The chirality of the SWNT is calculated by finding the vector **C** that is required to traverse the circumference of the tube. The vector can be expressed as a linear combination of the two basis vectors $\mathbf{a_1}$ and $\mathbf{a_2}$ of the hexagonal lattice of the graphene sheet as shown in Figure 4.1c. The chirality is represented as a pair integers (n, m) corresponding to the coefficients of the basis vectors. The specific chirality of a tube determines the electrical properties. The band structure of a carbon nanotube is related to that of a graphene sheet. For graphene, at the high symmetry points of the Brillouin zone, the conduction band touches the valence band, which results in a metallic

conductor. When the sheet is rolled up to form a SWNT, a quantization condition is introduced in the k-vector corresponding to the chiral vector. This requirement cuts sections of the graphene band diagram. These sections are the band structure of the SWNT. If one of the cuts passes through a high symmetry point where the bands touch, the nanotube has metallic conduction properties. Otherwise, it is a semiconductor. This condition can be expressed in terms of the basis vectors: if n-m is a multiple of three, then the tube is metallic, otherwise it has a band gap.

## 4.2 Fabrication Issues with CNT's

Integrating carbon nanotubes with top-down fabrication techniques entails particular challenges. In the first part of this section, we describe several CNT fabrication techniques and the difficulty in controlling chirality, length and tube orientation. In the next part we present some of our experimental studies on the damage of nanotubes by several standard fabrication techniques. These techniques were chosen because of their applicability to the goal of fabricating a resonator from a single carbon nanotube. We required that the device have low electrical resistance and that the nanotube be damaged as little as possible. Physical damage to the nanotube would lower the quality factor of the device.

### 4.2.1 Nanotube synthesis

There are several methods to fabricate CNT's that have been developed by researchers in the 1990's. Early methods include arc-discharge and laser ablation. In an arc-discharge process, an electrical arc is produced in a chamber between graphite electrodes, which supply the carbon for the nanotubes.[16] A small amount of transition-metal catalyst impurity is included in the graphite electrodes. The arc vaporizes the graphite, which deposits on the walls of the chamber in a variety of forms resembling soot. Certain regions of the deposit contain a high proportion of CNT's. The laser ablation method is similar to arc discharge, except that the graphite is vaporized by a laser pulse rather than an arc-discharge.[12] Both of these methods produce a high percentage of amorphous carbon, requiring the soot to be purified to yield high quality material. The purification process involves acids that may damage tubes.

In order to build devices, researchers made suspensions of the nanotubes by ultrasonic agitation in organic solvents. The suspension is then dropped onto a chip where the nanotubes, or bundles of nanotubes, stick to the surface by van der Walls forces. One of our goals was to conduct experiments on isolated SWNT's. It is very difficult to achieve a single SWNT with the suspension method. Additionally, we were able to make only poor electrical contacts to these tubes, possibly due to organic solvent adsorbed to the tubes.

More recently, a more subtle method has been developed for growing carbon nanotubes on a substrate by a chemical vapor deposition (CVD) method.[17] In this method, the substrate on which the CNT's are to be grown is seeded with catalytic material such as Fe or Ni. The substrate is placed into a high temperature tube furnace and a gaseous hydrocarbon such as methane or ethylene is flowed over the substrate. At

the high temperature, the hydrocarbon disassociates and the carbon dissolves in the metal catalyst, which becomes supersaturated with carbon. The carbon precipitates out of the particle as a carbon nanotube.[12] The CVD method is highly versatile. The catalyst can be patterned to create local regions from which CNT's grow. Varying the catalyst density can control the density of tubes, to the extreme case of dense "forests" of aligned nanotubes[18], under the right conditions. The selection of hydrocarbon and temperature allows one to grow either MWNT's or SWNT's. There are many variations on this technique. Patterned catalytic growth gives one some influence over the location and length of the nanotubes, though the chirality and orientation are still almost impossible to control.

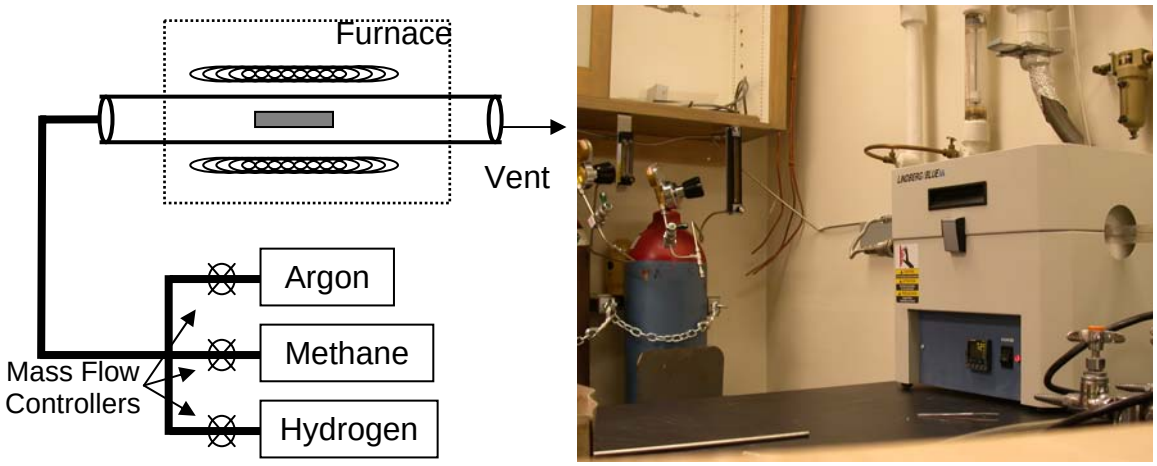


Figure 4.2: Left—schematic of tube nanotube synthesis system. Right—photograph of actual system with tube furnace and gas cylinders visible.

We found that the CVD synthesized tubes are more suitable than the arc-discharge or laser-ablation CNT's for fabricating the nanotube resonator. The nanotubes are of higher quality and it is easier to control the location of the nanotubes. Also, the

CVD method ensures that isolated tubes on the substrate are likely to truly be a single tube, not a small bundle of tubes. Finally, lower resistance electrical contacts were found in CVD synthesized tubes because they are cleaner with respect to solvents and amorphous carbon deposits.

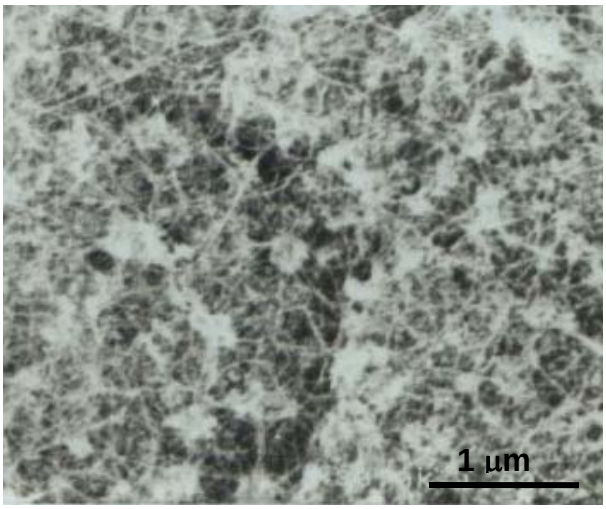


Figure 4.3: Film of SWNT's grown in CVD system of Figure 4.2.

We have set up a CVD tube furnace here at Caltech and grown carbon nanotubes using the patterned catalyst method. Figure 4.2, left, has a schematic of the CVD system while a photograph of the setup is shown on the right. The carbon feed stock is methane. Argon (Ar) is used as an inert gas when cooling or heating the system. Hydrogen ($H_2$) is added during heating to chemically reduce the catalyst and during CNT growth to reduce the amount of amorphous carbon that is produced in this process. In a typical process the tube furnace is heated to 900°C under Ar and $H_2$ flow at 500 $cm^3$/min and 2500 $cm^3$/min, respectively, after loading a sample that has been seeded with Fe catalyst. Once the furnace temperature has stabilized, the flow is switched to methane and hydrogen flow at

1500 $cm^3$/min each to grow the carbon nanotubes. After 5-15 minutes, the gas flow is switched back to argon flow at 1000 $cm^3$/min and the furnace is allowed to cool to room temperature. The growth time determines, to some degree, the length of the tubes synthesized. Figure 4.3 shows an SEM picture of a CNT film grown in this furnace. The process described above produces SWNT's; to grow MWNT's, replace the methane by acetylene and reduce the growth temperature to 800°C.

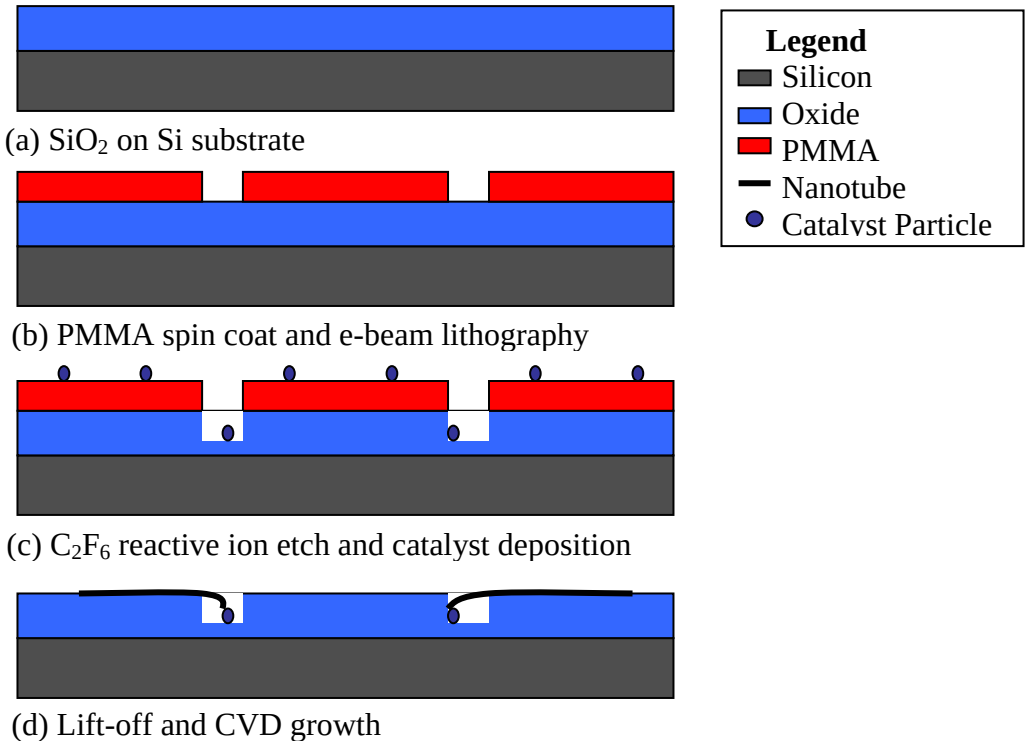


Figure 4.4: Patterned catalyst and nanotube growth procedure.

To conduct experiments on isolated SWNT's we developed a process to place small, isolated areas of catalyst on the surface. Figure 4.4 outlines the procedure, which begins with a silicon chip with thermally grown oxide on the surface. Electron beam lithography is performed on a layer of PMMA to define the areas where the catalyst will

be placed. A short reactive ion etch (RIE) is performed to create sunken sites. The chip is dipped into a solution of 1 mM $Fe(NO_3)_3 \bullet 9H_2O$ in isopropanol and then immediately dipped into hexane. The iron nitrate precipitates out in the hexane and deposits on the surface. An alternative method to deposit the catalyst is to evaporate a very thin film (less than 1 nm) of Fe and/or Ni. Next, the PMMA is stripped off with acetone, leaving the Fe catalyst in the indentations in the oxide. Finally, the chip is place into the CVD system to grow CNT's. Figure 4.5 shows tubes grown in this fashion. All the tubes in this AFM image originate in a hole in the surface where the catalyst was deposited.

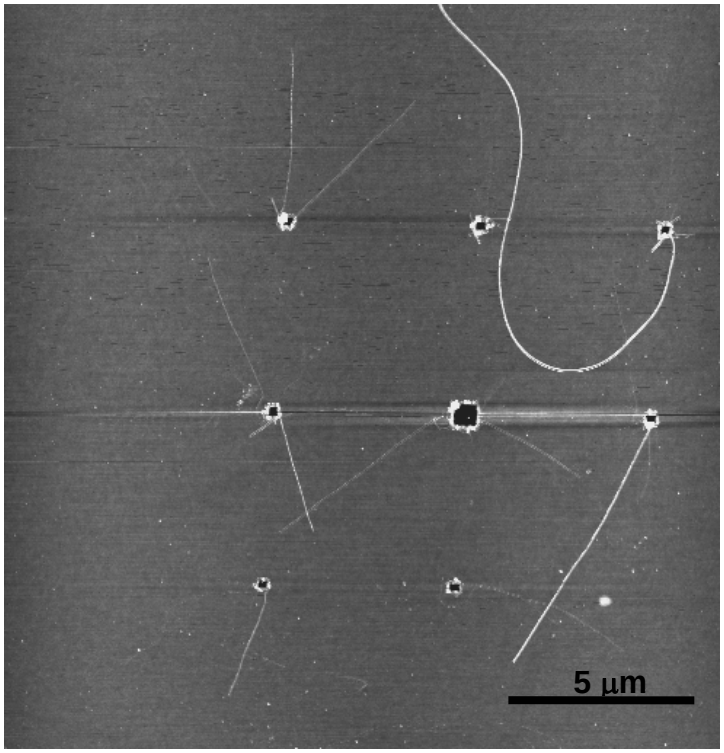


Figure 4.5: AFM image of nanotubes grown by patterned catalyst and CVD synthesis. All the nanotubes originate from catalyst particles in the holes.

Due to the high temperature process required to synthesize CNT's, it is challenging to integrate them with top-down fabricated structures. In order to place electrical contacts by electron beam lithography, for example, onto nanotubes, there must be some marks on the surface to align to. However, gold pads deposited before the synthesis will melt and deform in the tube furnace, an example of which is shown in Figure 4.6. Some methods around this particular problem are to deposit alignment marks after the furnace step or to use materials for alignment marks that will survive the high temperature growth. In particular, an iron alloy (trade name Kanthal), stable to 2000°C has been previously reported to be compatible with nanotube growth.[19]

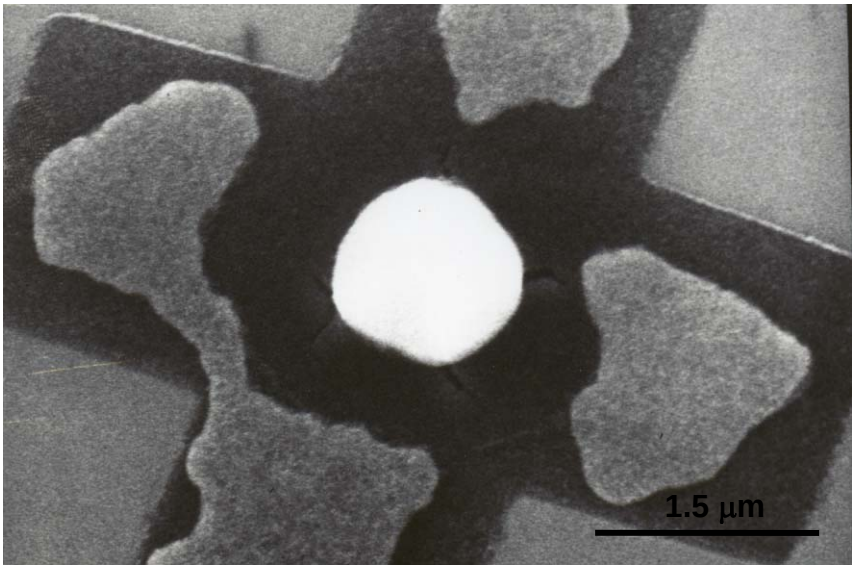


Figure 4.6: Gold alignment mark after CVD nanotube sythesis. The underlying chrome sticking layer shows the original shape of the alignment mark.

The approach we used was to fabricate alignment marks by sputtering of Kanthal. The nanotubes are imaged and mapped using atomic force microscopy (AFM) after synthesis. Electron beam lithography was used again to define the electrical leads.

Evaporation of Cr/Au and lift off complete the process of making electrical contacts to the carbon nanotubes. Stray conduction is minimized by the use of high quality thermally grown $SiO_2$ on Si wafers.

### 4.2.2 Fabrication effects on CNT's

Post-synthesis processing can pose a significant threat to the structural integrity or even survival of nanotubes. Damage from microfabrication techniques can reduce the conductivity and degrade the mechanical properties. As an example, Figure 4.7 shows an SEM picture of a carbon nanotube contacted by two metal pads and then subsequently subjected to a reactive ion etch (RIE) process, a common fabrication tool. The tube has been completely etched away where exposed.

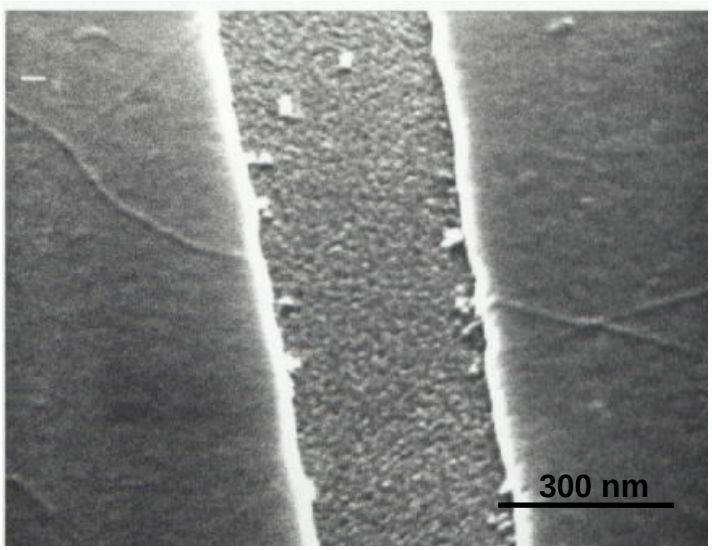


Figure 4.7: SEM picture of destroyed carbon nanotube after RIE etching.

In an attempt to characterize the damage done to CNT's by various fabrication techniques, the conductivity of the tube is taken as a proxy for the damage done by various microprocessing techniques. We made electrical contact, following the procedure outlined in previous chapters, to a collection of SWNT's fabricated using the CVD technique described in the previous section and measured the resistance of each. Next, the samples were subjected to common processing and etching techniques. At intervals, the effective resistances of the tubes were measured. An increase in resistance would indicate some form of damage to the tube.

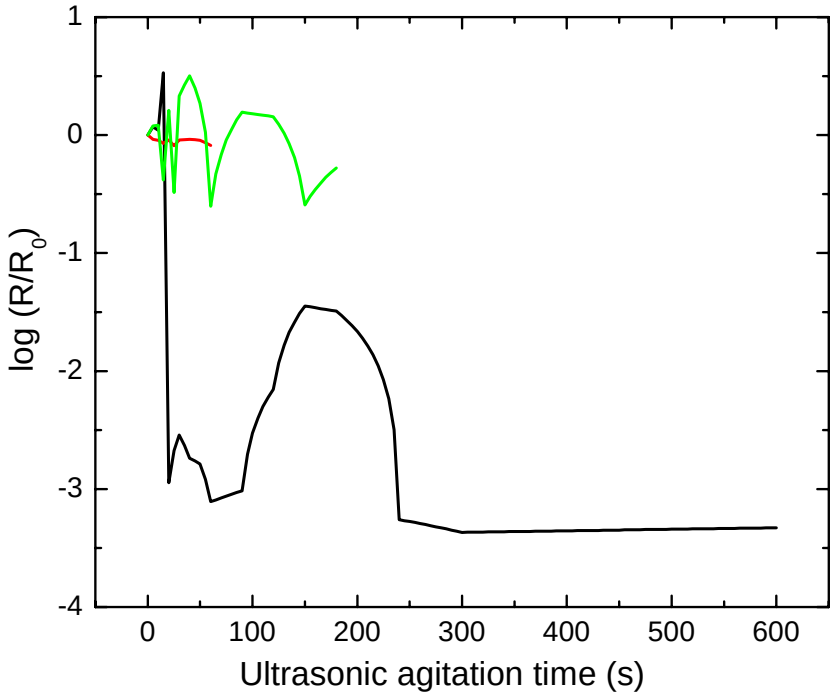


Figure 4.8: Relative change from original resistance $R_0$ vs. ultrasonic agitation time for three carbon nanotubes.

Ultrasonic agitation is often used to aid lift-off or as a helpful cleaning process in microfabrication. However, since the process involves the transmission of energy to the surface of the chip, it has the potential to damage small structures on the surface. To test

the effect of this process, a sample containing four SWNT's was prepared. The sample was agitated in acetone for 5 sec intervals, rinsed with isopropyl alcohol (IPA) and blown dry with nitrogen. The resistance of each tube was tested at each interval. Figure 4.8 plots the relative change in resistance vs. ultrasonic agitation time. One of the nanotubes did not survive any ultrasonic agitation and is not plotted here. Except for eventually losing contact or breaking, ultrasonic agitation has a relatively benign effect on nanotubes. A normal agitation time for fabrication is about 15 s, so we would expect to be able to use this process on nanotubes.

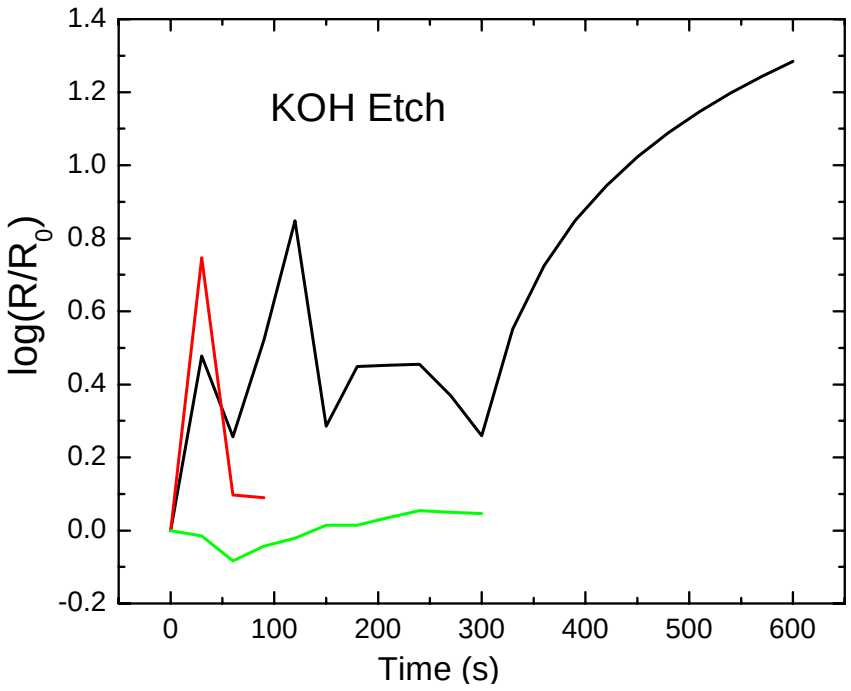


Figure 4.9: Resistance change vs. KOH Etch time for three carbon nanotubes.

The process described in the next section for creating a carbon nanotube resonator requires a sacrifical layer of sputtered Si to be etched away from under the nanotube, once it has been clamped. We tested three processes, all of which etch silicon, to

determine which would have the least impact on the nanotubes. Each will be described briefly and the data presented.

A solution of potassium hydroxide (KOH) is an anisotropic etch that preferentially exposes the (111) planes of single crystal Si. For sputtered Si, a 1 min etch removes 100 nm. A sample of four electrically contacted nanotubes was fabricated. The sample was dipped into 1M KOH solution for 30 s intervals, rinsed in deionized water and then IPA, and finally blown dry with nitrogen. The resistance of each tube was measured at each interval. The results are plotted in Figure 4.9. One of the four tubes did not survive any exposure to the etch. Etching in KOH clearly increases the resistance of tubes, which we interpret as damage.

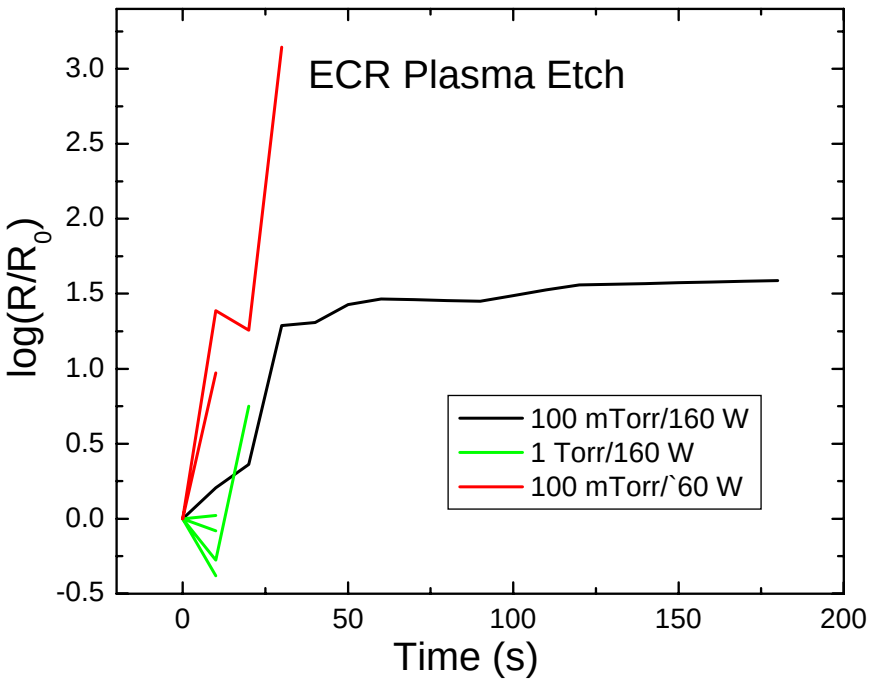


Figure 4.10: Resistance change vs. ECR etch time for various etch conditions.

Electron cyclotron resonance (ECR) etching is a type of low-pressure dry etch process which generates a plasma of molecules and ions that react with the material to be etched. The etch gas was $NF_3$. To etch 100 nm of Si, 20 s is required in this process. Three different conditions of pressure and input power were used on a total of eleven nanotubes for etch intervals of 10 s. The results are plotted in Figure 4.10. Some tubes did not survive at all and only three survived longer than 20 s. Plasma etch process are undoubtedly harmful to the integrity of carbon nanotubes.

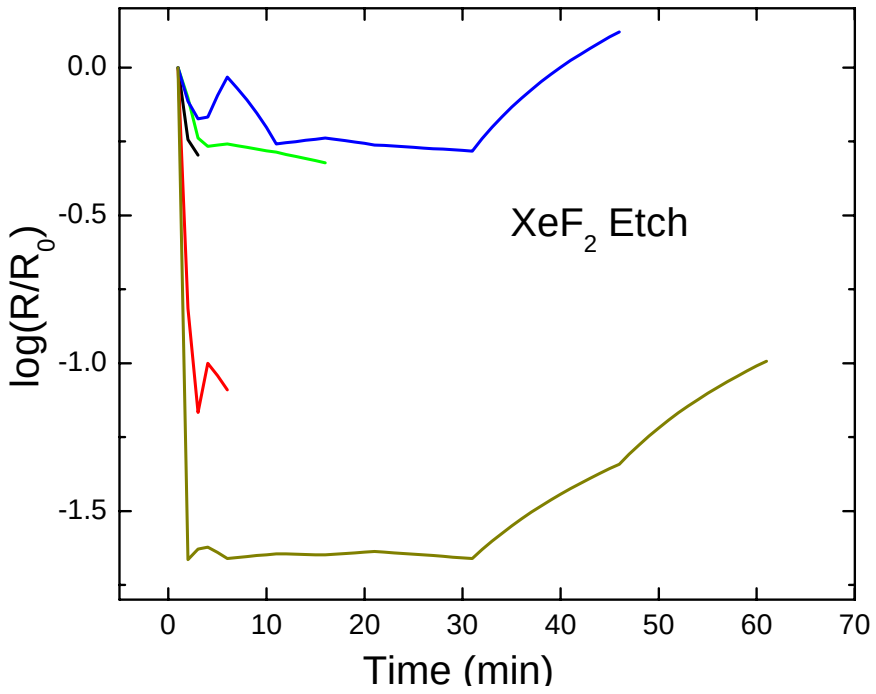


Figure 4.11: Resistance change vs. $XeF_2$ etch time for five carbon nanotubes.

The final etch technique tested was dry etching with $XeF_2$ in a low pressure chamber. This etch does not require a plasma, only heating to 80°C. The fluoride reacts with the Si, creating the volatile $SiF_4$, which is pumped away. This process is considerably slower, requiring 5-7 min to remove 100 nm of Si. Four of five tubes

survived the first interval of 5 min, shown in Figure 4.11. Interestingly, the conductivity of the tubes increases. This may be caused by adsorption of fluorine on the surface of the tubes. It has been previously reported that gas adsorption can influence the conduction properties of carbon nanotubes.[20] It is clear that dry etching with $XeF_2$ is the least damaging of the Si etch processes tested. In the next section, we make use of these results to design and carry out a process to create doubly-clamped carbon nanotube resonators.

## 4.3 Doubly-clamped carbon nanotube beam

Carbon nanotubes have many properties that lend them toward being used as ultra sensitive nanomechanical resonators. They have a large Young's modulus and a low density which is important for making high frequency, ultra-sensitive devices. In addition, because they are extremely resilient and can conduct charge, CNT's are an ideal material from which to fabricate electromechanical devices. We developed processes to fabricate and measure a single carbon nanotube resonator.

The CVD method was chosen for synthesizing nanotubes to fabricate into resonators because it offers cleaner, defect free material with low contact resistance. Figure 4.12 shows the fabrication process. A thermally grown $SiO_2$ on Si chip is prepared with a sputtered Si layer and Kanthal alignment marks. Carbon nanotubes are grown by the CVD method, and then mapped with an AFM. E-beam lithography, evaporation and lift-off create electrical contacts to candidate nanotubes. To complete the structure, the sample is etched in $XeF_2$, etching the sputtered Si layer and leaving a

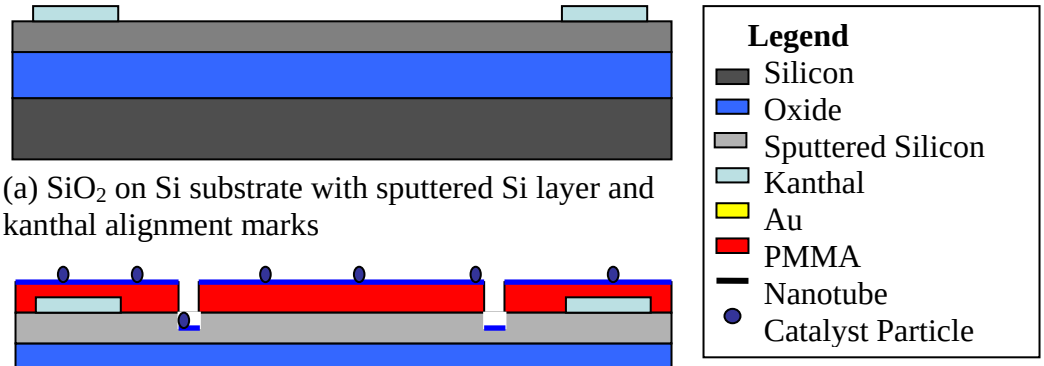


(a) $SiO_2$ on Si substrate with sputtered Si layer and kanthal alignment marks



(b) E-beam lithography, RIE and catalyst

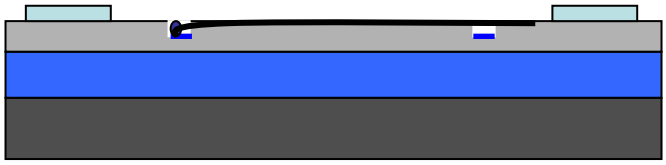

(c) Lift-off and CVD synthesis of nanotubes

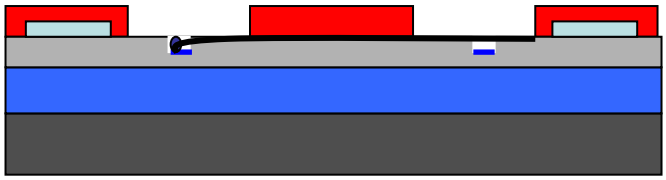

(d) E-beam lithography to define contacts

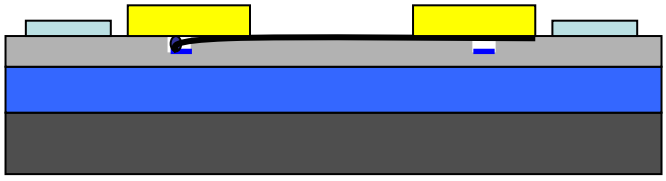

(e) Au evaporation and lift-off

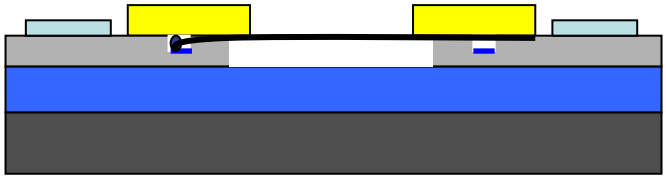

(f) XeF2 etch to undercut nanotube

Figure 4.12: Fabrication process to synthesize SWNT's and integrate them into doubly-clamped mechanical resonators.

freely suspended doubly-clamped carbon nanotube. Figure 4.13 shows an SEM image of a fabricated device.

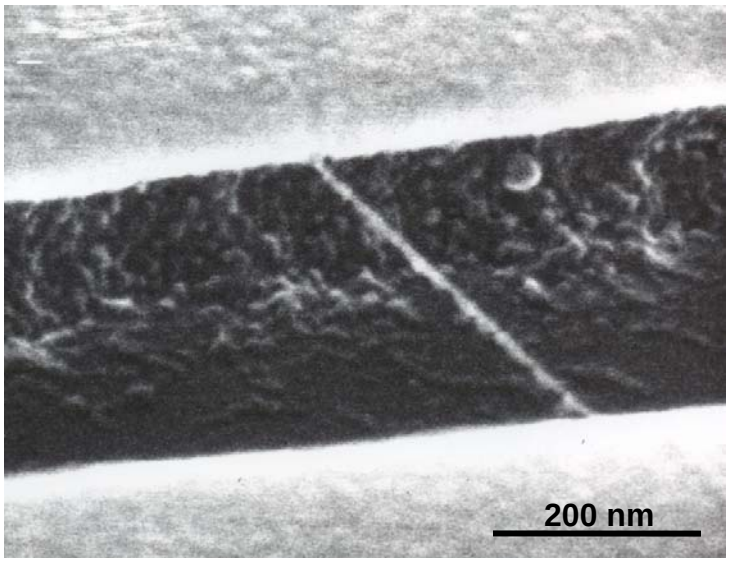


Figure 4.13: SEM image of doubly-clamped carbon nanotube beam.

We fabricated doubly-clamped carbon nanotube structures for measurement by the magnetomotive method described in Section 3.3. To accomplish such an experiment, the total input impedance at the device must be less than about 5 kΩ. However, single walled nanotubes have only a few quantum channels to conduct electrons. Each quantum channel has conductance $2e^2/h$, or about 13 kΩ. In the absence of any other scattering or contact resistance, two quantum channels have a resistance of 6.5 kΩ out of range to directly drive from the RF source. Even with the 50 Ω terminations, as shown in Figure 3.4, the output signal would be divided down to lower power than the noise introduced by the output amplifier. One method to measure a SWNT magnetomotively would be to design a matching circuit composed of capacitive and inductive elements. The matching circuit is impractical for this purpose, however. A single stage matching circuit has a

very narrow pass band and the frequency of the device, though it can be calculated approximately, is not known *a priori*. Another method would be to fabricate two CNT resonators in an electrical bridge configuration, with a null voltage at the common terminal. Then a change in impedance of one or other branches of the bridge will result in a non-zero voltage at the common terminal. Yet another possible method is to use the nanotube as both a resonator and a single-electron-transistor (SET) for detection.[21]

We did not achieve measurements on this device due to the difficult fabrication process and very small yield of low resistance samples. This project is ongoing with collaborators making efforts to fabricate and measure both SWNT and MWNT nanotube resonators magnetomotively.

## 4.4 Field-emission with integrated grid

We collaborated with the Submillimeter Wave Advanced Technology (SWAT) group at Jet Propulsion Laboratory (JPL) to fabricate electron field emission sources for miniature mass spectrometers and the nanoklystron. JPL has a program to develop miniature mass spectrometers for chemical analysis in space exploration and environmental monitoring for astronaut safety. A key component of a miniature mass spectrometer is an electron beam to ionize the molecules being analyzed. The nanoklystron is an effort under way at JPL to create a terahertz radiation source, which involves an electron resonance chamber at the frequency of interest.[22] The nanoklystron is designed for space applications, specifically for elemental analysis. A key requirement of this project is a nanoscale field emission source that can be integrated into the package.

The specifications for the source are particularly rigorous requiring a current density of 1 $kA/cm^2$ and a low operating voltage

Carbon nanotubes, in addition to its other outstanding properties, are one of the best materials for generating free electrons through field emission. Table 1 compares the electric field strength required for emission for a variety of materials—CNT's being the lowest.[15] In addition, CNT's have other properties suitable for field emission. Tubes are extremely stable, and therefore have the potential for long life as field emitters. The physical structure of CNT's also brings benefits. When a voltage is applied to a metallic object, electric field lines concentrate at surfaces with a very small radius of curvature. SWNT's can have a radius as small as .7 nm, yielding very high field amplification at the tips.

| Material | Threshold electric field (V/μm) |
|---|---|
| Mo tips | 50-100 |
| Si tips | 50-100 |
| p-type semiconducting diamond | 130 |
| Undoped, defective CVD diamond | 30-120 |
| Amorphous diamond | 20-40 |
| Cs-coated diamond | 20-30 |
| Graphite powder(<1mm size) | 17 |
| Nanostructured diamond | 3-5 |
| Carbon nanotubes | 1-3 |

Table 4.1: Field emission threshold for various materials.[23]

Single-walled carbon nanotube films grown with the CVD system described in Section 4.2.1 were fabricated on degenerately doped silicon wafers in order to make

electrical contact to the tubes. This sample was tested for field emission along with CVD tubes synthesized by Hoenk at JPL and by Baohe at Brown University. The JPL nanotubes were disordered MWNT's while the samples from Brown were ordered MWNT's grown in an anodized alumina template. The samples were tested in an ultra-high vacuum (UHV) system with pressure of 1 x $10^{-10}$ torr. The anode was spaced 1 μm away from the sample chip surface. Figure 4.14 shows the current emission density as a function of the electric field. The Caltech sample has the highest threshold electric field and emits a lower current density than the other samples. It is apparent that our nanotubes are not as efficient as field emitters as others. This may have been because of a lower density of emitters on the surface, or poor contact between the substrate and nanotubes. In addition, arcing within the chamber damaged our sample as shown in the SEM image of Figure 4.15.

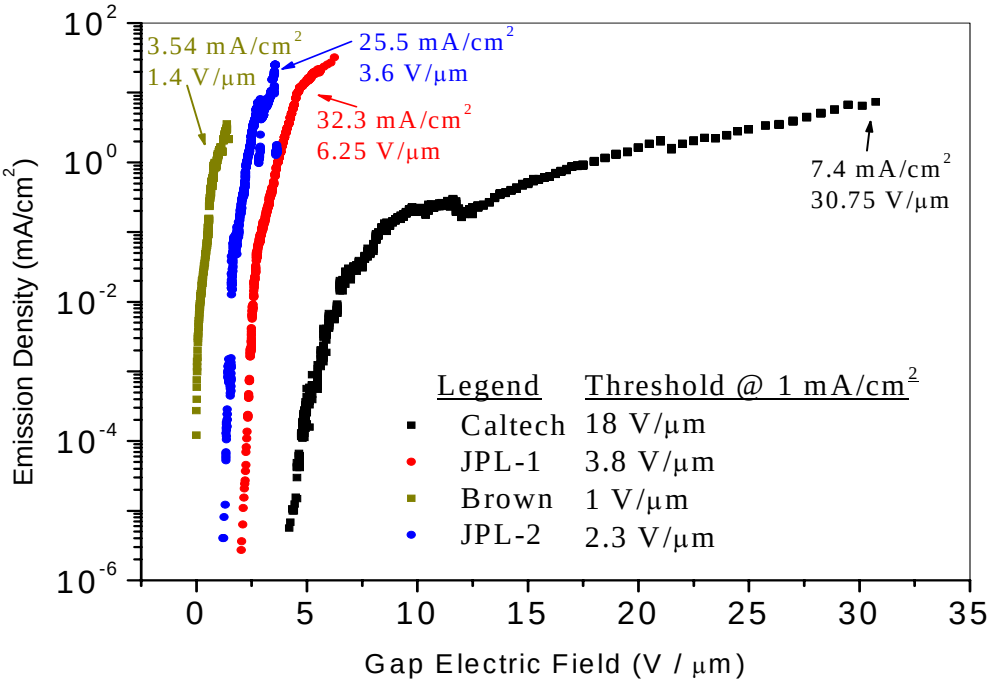


Figure 4.14: Emission current density vs. electric field for nanotubes fabricated by JPL, Brown University and Caltech with the threshold voltage tabulated for each sample.

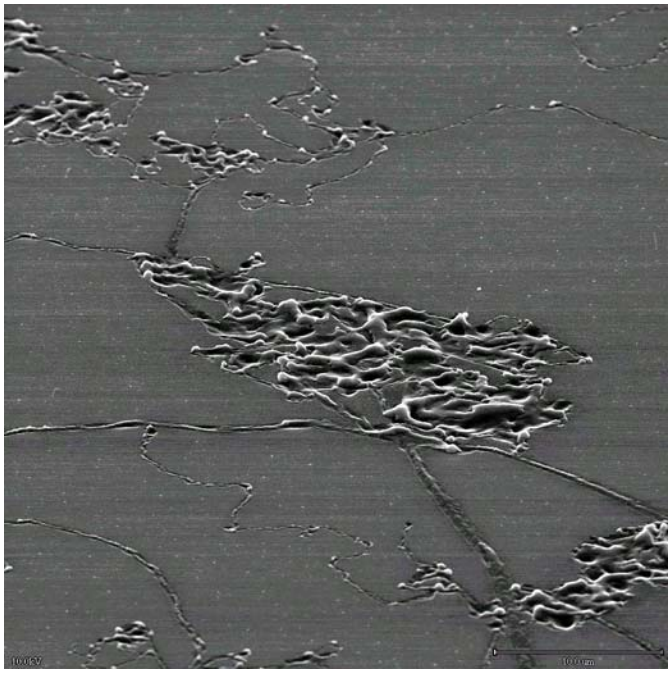

Figure 4.15: SEM image of pitted surface of SWNT field emission sample from arcing within test chamber.

Because of the cost of extra weight in space applications, a critical requirement is that the device operates at low voltage. To minimize the voltage, the anode must be as close to the field emission source as possible. We have designed and a method of integrating a grid onto CVD grown carbon nanotubes and fabricated such structures. Though our tubes don't seem to be the optimal for the nanoklystron, we used them for the integrated grid structure for the purposes of proof of concept.

Figure 4.16 shows the process steps for making the integrated grid structure. The process begins with a disordered mat of SWNT's synthesized on a degenerately n-doped silicon wafer by the process described above. The degenerate Si allows us to have electrical contact to the nanotube from the backside of the chip. Next, the nanotubes are

encased in amorphous Si deposited by sputtering which protects the tubes and sets the gap between the anode and the nanotubes (cathode). Finally, an Au layer of 100 nm is evaporated on top of the sputtered Si. Electron-beam lithography is used to define a grid structure which is transferred to the Au layer by ion beam milling. The tubes are finally exposed by etching the sputtered Si away. This also leaves a suspended, integrated metal grid to extract electrons.

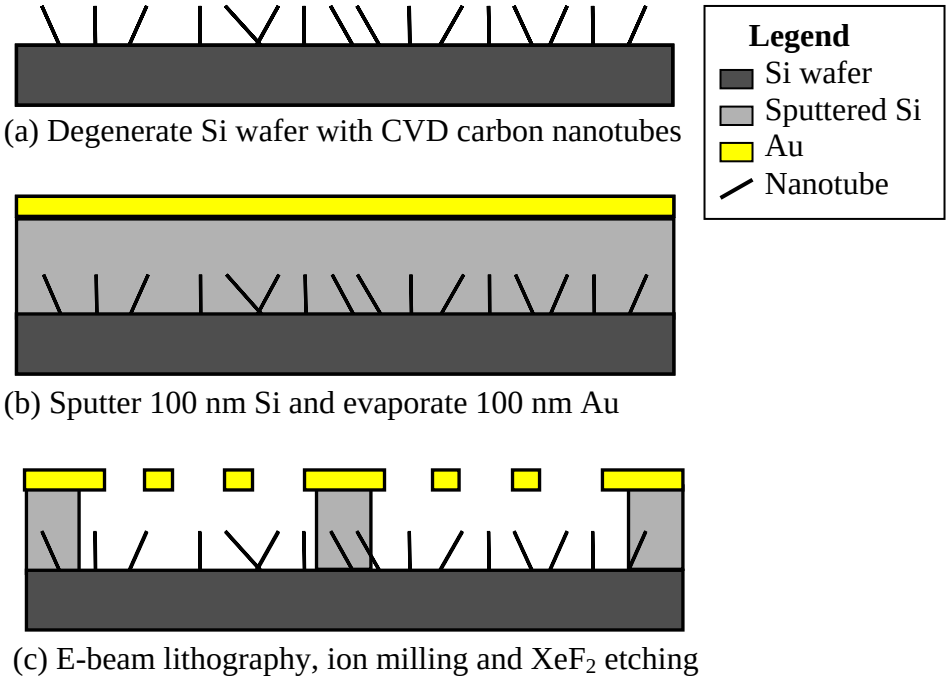


(a) Degenerate Si wafer with CVD carbon nanotubes

(b) Sputter 100 nm Si and evaporate 100 nm Au

(c) E-beam lithography, ion milling and $XeF_2$ etching

Figure 4.16: Fabrication of integrated grid above CVD grown carbon nanotubes.

The design of the grid involves some trade-offs. The strength and durability of the suspended grid increases as the size of the holes decreases, for a particular lattice constant. This is desirable for the purpose of structural integrity. However, the grid will collect some of the electrons emitted from the carbon nanotube film. Larger grid holes leave less area filled by the grid, and therefore less electrons collected. The fill factor of

the grid will be optimized in future generations of the device. Possibly the most efficient grid structure will lie below the field emission tips.

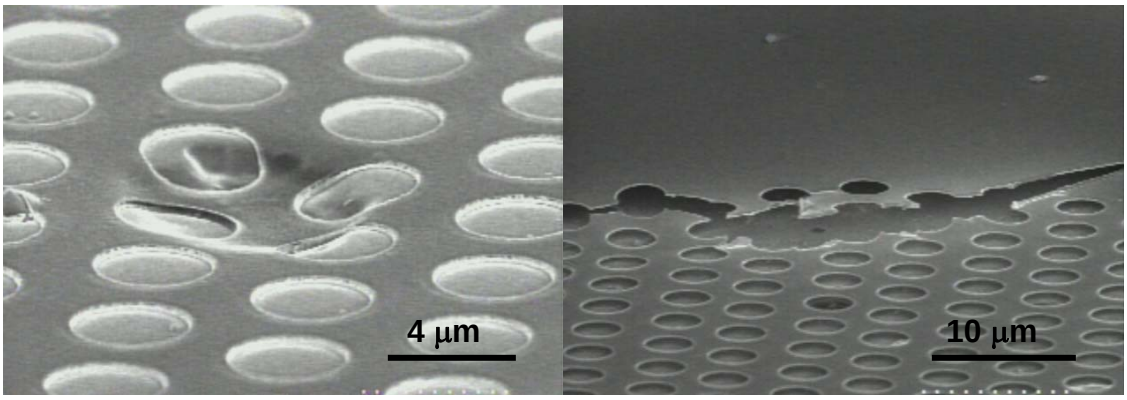


Figure 4.17: SEM images of buckled and torn grids for CNT field emission device.

An issue that has arisen in this process is stress within the evaporated gold layer. Figure 4.17 shows SEM pictures of a buckled and broken grid structures. Grids damaged in this way are not usable because they are shorted to the nanotubes or the degenerate Si wafer. A thicker gold layer may be more stiff and robust to avoid this problem. Also, the holes were close enough together that the grid was completely undercut by the isotropic $XeF_2$ etch. Eliminating grid holes in a few locations would create supports for the grid as shown in Figure 4.16c.

Some samples were successfully fabricated with integrated grids as shown in the SEM images of Figure 4.18. Unfortunately, all samples that were loaded into the vacuum chamber were not testable because the grid became shorted to the chip. Figure 4.19 shows the sample after being removed from the vacuum chamber. For some reason, the grids collapse within the test setup, perhaps from vibrations of the chamber during pumping. The next generation will use a thicker metal grid layer for increased stability

and robustness. As of this writing, collaborators Dr. Harish Manohara of JPL and undergraduate Wei Dang of Caltech are continuing to fabricate and test these types of structures for the nanoklystron.

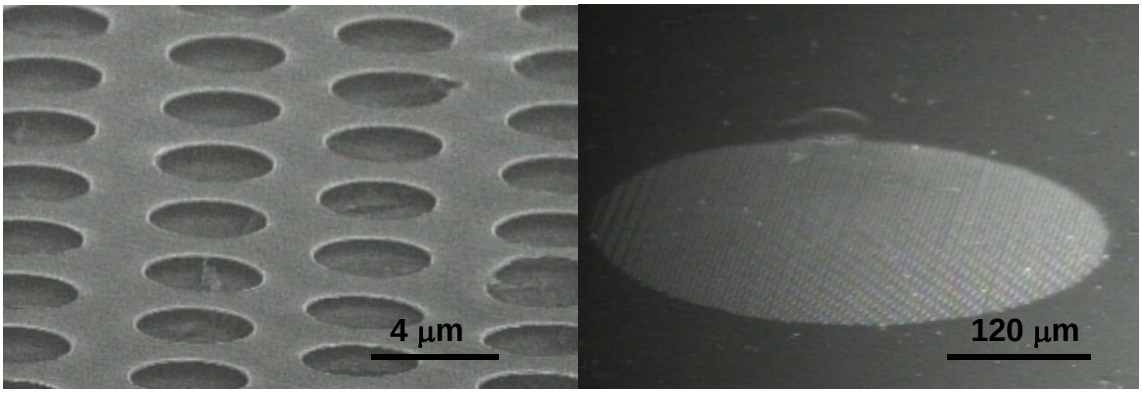


Figure 4.18: SEM images of completed CNT field emission device with integrated grid.

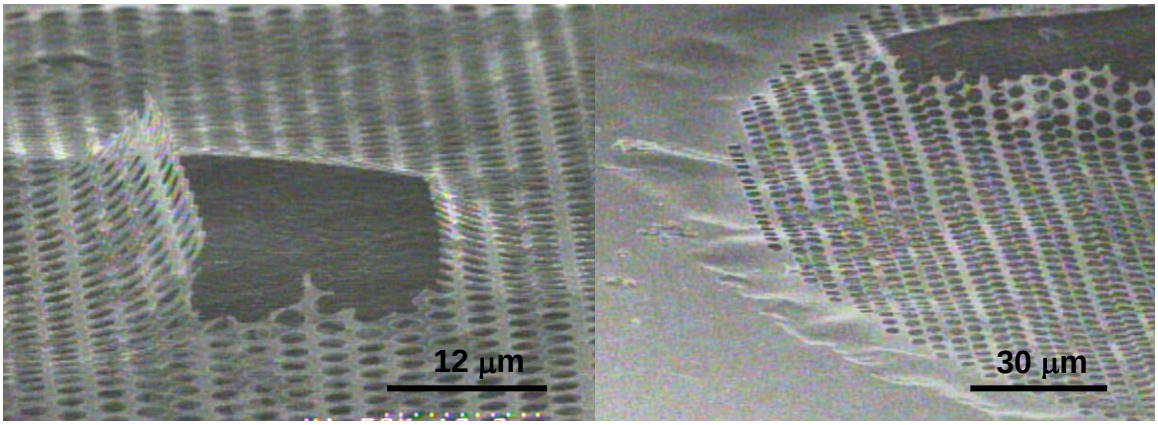


Figure 4.19: SEM images of damaged grids after testing attempt. It is not know exactly when this damage occurred.

## 4.5 Summary

In this work we have characterized the effects of various microfabrication processes on the conductivity of carbon nanotubes for the purpose of fabricating high-Q nanomechanical resonators. Of the Si etches tested, $XeF_2$ was found to be the least damaging, while plasma etch processes were the most destructive. Doubly-clamped CNT resonators were fabricated, though not tested. Nanotubes were also explored for field emission and a novel design for integrated extraction grids was fabricated. Both the latter projects are still being pushed forward by collaborators.

# References


[1] S. Iijima, "Helical microtubules of graphitic carbon," *Nature* **354** (6348), 56-58 (1991).

[2] S. Iijima and T. Ichihashi, "Single-shell carbon nanotubes of 1 nm diameter," *Nature* **363** (6430), 603-605 (1993).

[3] D. S. Bethune, C. H. Kiang, M. S. de Vries et al., "Cobalt-catalyzed growth of carbon nanotubes with single-atomic-layer walls," *Nature* **363** (6430), 605-607 (1993).

[4] H. Y. Peng, N. Wang, Y. F. Zheng et al., "Smallest diameter carbon nanotubes," *Applied Physics Letters* **77** (18), 2831-2833 (2000).

[5] S. J. Tans, A. R. M. Verschueren, and C. Dekker, "Room-temperature transistor based on a single carbon nanotube," *Nature* **393** (6680), 49-52 (1998).

[6] H. W. Ch. Postma, T. Teepen, Z. Yao et al., "Carbon nanotube single-electron transistors at room temperature," *Science* **293** (5527), 76-79 (2001).

[7] H. J. Dai, J. H. Hafner, A. G. Rinzler et al., "Nanotubes as nanoprobes in scanning probe microscopy," *Nature* **384** (6605), 147-150 (1996).

[8] P. A. Williams, S. J. Papadakis, A. M. Patel et al., "Fabrication of nanometer-scale mechanical devices incorporating individual multiwalled carbon nanotubes as torsional springs," *Applied Physics Letters* **82** (5), 805-807 (2003).

[9] A. N. Kolmogorov and V. H. Crespi, "Smoothest bearings: Interlayer sliding in multiwalled carbon nanotubes," *Physical Review Letters* **85** (22), 4727-4730 (2000).

[10] T. Rueckes, K. Kim, E. Joselevich et al., "Carbon nanotube-based nonvolatile random access memory for molecular computing," *Science* **289** (5476), 94-97 (2000).

[11] H. W. Kroto, J. R. Heath, S. C. O'Brien et al., "C-60 - Buckminsterfullerene," *Nature* **318** (6042), 162-163 (1985).

[12] A. Thess, R. Lee, P. Nikolaev et al., "Crystalline ropes of metallic carbon nanotubes," *Science* **273** (5274), 483-487 (1996).

[13] M. M. J. Treacy, T. W. Ebbesen, and J. M. Gibson, "Exceptionally high Young s modulus observed for individual carbon nanotubes," *Nature* **381** (6584), 678-680 (1996).

[14] P. G. Collins and P. Avouris, "Nanotubes for electronics," *Scientific American* **283** (6), 62 (2000).

[15] J. M. Bonard, H. Kind, T. Stockli et al., "Field emission from carbon nanotubes: the first five years," *Solid-state Electronics* **45** (6), 893-914 (2001).

[16] T. W. Ebbesen and P. M. Ajayan, "Large-scale synthesis of carbon nanotubes," *Nature* **358** (6383), 220-222 (1992).

[17] J. Kong, H. T. Soh, A. M. Cassell et al., "Synthesis of individual single-walled carbon nanotubes on patterned silicon wafers," *Nature* **395** (6705), 878-881 (1998).

[18] S. S. Fan, M. G. Chapline, N. R. Franklin et al., "Self-oriented regular arrays of carbon nanotubes and their field emission properties," *Science* **283** (5401), 512-514 (1999).

[19] J. M. Bonard, T. Stockli, O. Noury et al., "Field emission from cylindrical carbon nanotube cathodes: Possibilities for luminescent tubes," *Applied Physics Letters* **78** (18), 2775-2777 (2001).

[20] J. Kong, N. R. Franklin, C. W. Zhou et al., "Nanotube molecular wires as chemical sensors," *Science* **287** (5453), 622-625 (2000).

[21] S. Sapmaz, Y. M. Blanter, L. Gurevich et al., "Carbon nanotubes as nanoelectromechanical systems," *Physical Review. B, Condensed Matter and Materials Physics* **67** (23), art.no.-235414 (2003).

[22] P. H. Siegel, T. H. Lee, and J. Xu, ""The Nanoklystron: A new concept for THz power generation," *JPL New Technology Report* (2000).

[23] M. S. Dresselhaus, G. Dresselhaus, and Phaedon Avouris, *Carbon nanotubes : synthesis, structure, properties, and applications*. (Springer, Berlin ; New York, 2001), pp.xv, 447.